Inorg. Chem. **2008**, *47*, 6796−6803

Photophysics of the Platinum(II) Terpyridyl Terpyridylacetylide Platform and the Influence of Fe^{II} and Zn^{II} Coordination

Maria L. Muro,[†] Stéphane Diring,[‡] Xianghuai Wang,[†] Raymond Ziessel,*[,‡] and Felix N. Castellano*[,†]

Department of Chemistry and Center for Photochemical Sciences, Bowling Green State University, Bowling Green, Ohio 43403, and Laboratoire de Chimie Moléculaire associé au Centre National de la Recherche Scientifique (LCM-CNRS), Ecole de Chimie, polymères, Matériaux (ECPM), 25 rue Becquerel, 67087 Strasbourg Cedex, France

Received February 19, 2008

The synthesis, structural characterization, and photoluminescence (PL) properties of the square-planar terpyridylplatinum(II) complex $[^tBu_3tpyPtCCtpy]^+$ (**1**) and the octahedral trinuclear Fe^{II} and Zn^{II} analogues $[Fe(^tBu_3tpyPtCCtpy)_2]^{4+}$ (**2**) and $[Zn(^tBu_3tpyPtCCtpy)_2]^{4+}$ (**3**) are described. The photophysical properties of the mononuclear Pt^{II} complex **1** are consistent with a charge-transfer excited-state parentage producing a large Stokes shift with a concomitant broad, structureless emission profile. The Fe-based ligand-field states in **2** provide an efficient nonradiative deactivation pathway for excited-state decay, resulting in a nonemissive compound at room temperature. Interestingly, upon chelation of **1** with Zn^{II}, a higher energy charge-transfer emission with a low-energy shoulder and a 215 ns excited-state lifetime is produced in **3**. A spectroscopically identical species relative to **3** was produced in control experiments when **1** was reacted with excess protons ($HClO_4$) as ascertained by UV−vis and static PL spectra measured at room temperature and 77 K. Therefore, the chelation of Zn^{II} to **1** is acid−base in nature, and its Lewis acidity renders the highest occupied molecular orbital level in **1** much less electron-rich, which induces a blue shift in both the absorption and emission spectra. At 77 K, complexes **1**, **3**, and protonated **1** display at least one prevalent vibronic component in the emission profile (1360 cm^{-1}) resembling PL emanating from a ligand-localized excited-state, indicating that these emitting states are inverted relative to room temperature. These results are qualitatively confirmed by the application of time-dependent theory using only the 1360 cm^{-1} mode to reproduce the low-temperature emission spectra.

Introduction

The development of square-planar platinum(II) complexes containing polypyridyl ligands has increased over the past decade largely because of the impressive photophysical properties displayed by these compounds. The presence of low-energy absorption bands, long-lived excited states, high-photoluminescence (PL) quantum yields have made these complexes suitable for comprehensive fundamental studies[1–20] as well as for a variety of applications such as light-emitting materials,[21,22] photocatalysis and hydrogen production,[23,24] dye-sensitized solar cells,[25,26] biosensors,[27,28] photoswitches,[29] excited-state electron transfer,[30] singlet oxygen sensitization,[31] and optical limiting materials.[32] A notable facet of these structures relates to the concept that

* To whom correspondence should be addressed. E-mail: ziessel@chimie.u-strasbg.fr (R.Z.), castell@bgsu.edu (F.N.C.).
† Bowling Green State University.
‡ LCM-CNRS, ECPM.

(1) Castellano, F. N.; Pomestchenko, I. E.; Shikhova, E.; Hua, F.; Muro, M. L.; Rajapakse, N. *Coord. Chem. Rev.* **2006**, *250*, 1819–1828.
(2) Hissler, M.; Connick, W. B.; Geiger, D. K.; McGarrah, J. E.; Lipa, D.; Lachicotte, R. J.; Eisenberg, R. *Inorg. Chem.* **2000**, *39*, 447–457.
(3) Shikhova, E.; Danilov, E. O.; Kinayyigit, S.; Pomestchenko, I. E.; Tregubov, A. D.; Camerel, F.; Retaileau, P.; Ziessel, R.; Castellano, F. N. *Inorg. Chem.* **2007**, *46*, 3038–3048.
(4) Whittle, C. E.; Weinstein, J. A.; George, M. W.; Schanze, K. S. *Inorg. Chem.* **2001**, *40*, 4053–4062.
(5) Arena, G.; Calogero, G.; Campagna, S.; MonsuScolaro, L.; Ricevuto, V.; Romeo, R. *Inorg. Chem.* **1998**, *37*, 2763–2769.
(6) Crites, D. K.; McMillin, D. R. *Coord. Chem. Rev.* **2001**, *211*, 195–205.
(7) Danilov, E. O.; Pomestchenko, I. E.; Kinayyigit, S.; Gentili, P. L.; Hissler, M.; Ziessel, R.; Castellano, F. N. *J. Phys. Chem. A* **2005**, *109*, 2465–2471.
(8) Hua, F.; Kinayyigit, S.; Cable, J. R.; Castellano, F. N. *Inorg. Chem.* **2005**, *44*, 471–473.
(9) Hua, F.; Kinayyigit, S.; Cable, J. R.; Castellano, F. N. *Inorg. Chem.* **2006**, *45*, 4304–4306.

10.1021/ic800316x CCC: $40.75
Published on Web 07/08/2008

their excited-state properties are easily tuned through alteration of the electronic structure of the ligands attached to the Pt^{II} center.

Generally speaking, many Pt^{II} complexes studied to date can be considered end-capped, thereby limiting the possibility of structural expansion and hence the formation of more complex polynuclear systems. Attachment of pendant ligands to the Pt^{II} center will certainly open the possibility of generating heteronuclear complexes with the opportunity of studying the resultant photophysical properties of these new polymetallic systems. The present work investigates how coordination of Fe^{II} and Zn^{II} to pendant terpyridylacetylide units fused to a platinum(II) terpyridyl complex (**1**) influences its photophysical properties. Zn^{II} was selected based on the premise that it would not become electronically involved in either ground-state behavior or excited-state decay. However, it would serve the role of a Lewis acid to template an octahedral environment where the terpyridyl-based ligand-localized photophysics could be explored, thereby simulating the chemical/electronic environment resulting from Fe^{II} coordination. The selection of Fe^{II} arose from two independent reports out of the Schmehl and Brewer laboratories where the presence of iron did not adversely affect the photophysics of their respective systems. In the former work, a trinuclear complex of the topology Ru−Fe−Ru bridged through phenylenevinylene-substituted diimine ligands produces a long-lived ligand-localized triplet state (^{3}IL).[33] Brewer and co-workers[34] also demonstrated how attached aromatic chromophores such as anthracene, electronically decoupled from the metal center, are able to retain their ligand-based singlet emission properties even in the presence of the deactivating iron center. To the best of our knowledge, these are the only Fe^{II} complexes reported with excited-state lifetimes surpassing ultrafast time scales. Herein, we report the photophysical properties of the terpyridylplatinum(II) complexes: [^{t}Bu$_3$tpyPtC≡Ctpy]$^+$ (**1**), where ^{t}Bu$_3$tpy = 4,4′,4″-tri-*tert*-butyl-2,2′:6′,2″-terpyridine and its corresponding Fe^{II} and Zn^{II} analogues, [Fe(^{t}Bu$_3$tpyPtC≡Ctpy)$_2$]$^{4+}$ (**2**) and [Zn(^{t}Bu$_3$tpyPtC≡Ctpy)$_2$]$^{4+}$ (**3**).

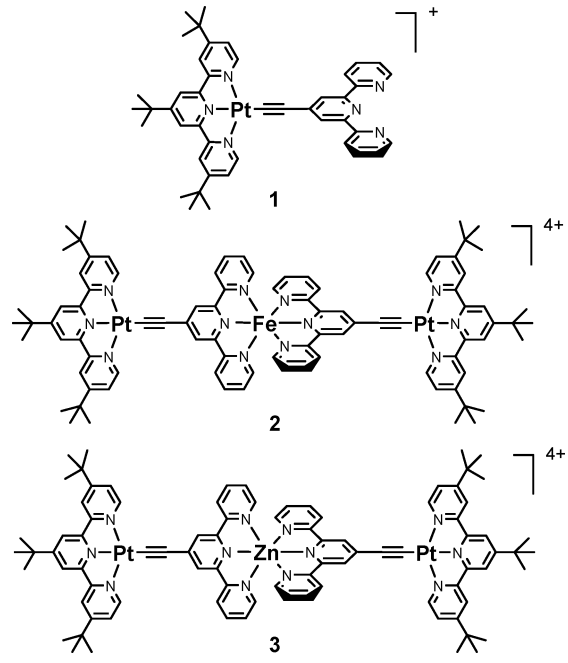

Experimental Section

General Procedures and Materials. The complexes used in this work were obtained using synthetic procedures that have already been reported.[35] [(^{t}Bu$_3$tpy)PtCl]Cl[20] and 4-ethynyl-2,2′:6′,6″-terpyridine[36] were prepared according to previously described procedures. $Fe(ClO_4)_2 \cdot 6H_2O$ was obtained from Alfa Aesar and used without further purification. $Zn(ClO_4)_2 \cdot 6H_2O$ was purchased from Aldrich Chemical Co. and used as received. The titration experiments were carried out under an argon atmosphere, and the titrations were performed several times using freshly prepared solutions each time.

[^{t}Bu$_3$tpyPtC≡Ctpy]BF$_4$ (1). [(^{t}Bu$_3$tpy)PtCl]Cl (0.163 g, 0.244 mmol) was dissolved in a mixture of *N*,*N*-dimethylformamide

(10) Jude, H.; Bauer, J. A. K.; Connick, W. B. *Inorg. Chem.* **2004**, *43*, 725–733.
(11) McMillin, D. R.; Moore, J. J. *Coord. Chem. Rev.* **2002**, *229*, 113–121.
(12) Michalec, J. F.; Bejune, S. A.; Cuttell, D. G.; Summerton, G. C.; Gertenbach, J. A.; Field, J. S.; Haines, R. J.; McMillin, D. R. *Inorg. Chem.* **2001**, *40*, 2193–2200.
(13) Michalec, J. F.; Bejune, S. A.; McMillin, D. R. *Inorg. Chem.* **2000**, *39*, 2708–2709.
(14) Miskowski, V. M.; Houlding, V. H.; Che, C. M.; Wang, Y. *Inorg. Chem.* **1993**, *32*, 2518–2524.
(15) Moore, J. J.; Nash, J. J.; Fanwick, P. E.; McMillin, D. R. *Inorg. Chem.* **2002**, *41*, 6387–6396.
(16) Pomestchenko, I. E.; Castellano, F. N. *J. Phys. Chem. A* **2004**, *108*, 3485–3492.
(17) Pomestchenko, I. E.; Luman, C. R.; Hissler, M.; Ziessel, R.; Castellano, F. N. *Inorg. Chem.* **2003**, *42*, 1394–1396.
(18) Williams, J. A. G.; Beeby, A.; Davies, E. S.; Weinstein, J. A.; Wilson, C. *Inorg. Chem.* **2003**, *42*, 8609–8611.
(19) Wong, K. M.-C.; Tang, W.-S.; Lu, X.-X.; Zhu, N.; Yam, V. W.-W. *Inorg. Chem.* **2005**, *44*, 1492–1498.
(20) Yip, H.-K.; Cheng, L.-K.; Cheung, K.-K.; Che, C.-M. *J. Chem. Soc., Dalton Trans.* **1993**, 2933–2938.
(21) Chan, S.-C.; Chan, M. C. W.; Wang, Y.; Che, C.-M.; Cheung, K.-K.; Zhu, N. *Chem.—Eur. J.* **2001**, *7*, 4180–4190.
(22) Lu, W.; Mi, B.-X.; Chan, M. C. W.; Hui, Z.; Che, C.-M.; Zhu, N.; Lee, S.-T. *J. Am. Chem. Soc.* **2004**, *126*, 4958–4971.
(23) Du, P.; Schneider, J.; Jarosz, P.; Eisenberg, R. *J. Am. Chem. Soc.* **2006**, *128*, 7726–7727.
(24) Narayana-Prabhu, R.; Schmehl, R. H. *Inorg. Chem.* **2006**, *45*, 4319–4321.
(25) Geary, E. A. M.; Yellowlees, L. J.; Jack, L. A.; Oswald, I. D. H.; Parsons, S.; Hirata, N.; Durrant, J. R.; Robertson, N. *Inorg. Chem.* **2005**, *44*, 242–250.
(26) Islam, A.; Sugihara, H.; Hara, K.; Singh, L. P.; Katoh, R.; Yanagida, M.; Takahashi, Y.; Murata, S.; Arakawa, H.; Fujihashi, G. *Inorg. Chem.* **2001**, *40*, 5371–5380.
(27) Ratilla, E. M. A.; Brothers, H. M.; Kostic, N. M. *J. Am. Chem. Soc.* **1987**, *109*, 4592–4599.
(28) Wong, K. M.-C.; Tang, W.-S.; Chu, B. W.-K.; Zhu, N.; Yam, V. W.-W. *Organometallics* **2004**, *23*, 3459–3465.
(29) Yutaka, T.; Mori, I.; Kurihara, M.; Mizutani, J.; Tamai, N.; Kawai, T.; Irie, M.; Nishihara, H. *Inorg. Chem.* **2002**, *47*, 7143–7150.
(30) Cortes, M.; Carney, J. T.; Oppenheimer, J. D.; Downey, K. E.; Cummings, S. D. *Inorg. Chim. Acta* **2002**, *333*, 148–151.
(31) Zhang, D.; Wu, L.-Z.; Yang, Q.-Z.; Li, X.-H.; Zhang, L.-P.; Tung, C.-H. *Org. Lett.* **2003**, *5*, 3221–3224.
(32) Guo, F.; Sun, W.; Liu, Y.; Schanze, K. *Inorg. Chem.* **2005**, *44*, 4055–4065.
(33) Baitalik, S.; Wang, X.-Y.; Schmehl, R. H. *J. Am. Chem. Soc.* **2004**, *126*, 16304–16305.
(34) Zigler, D. F.; Elvington, M. C.; Heinecke, J.; Brewer, K. J. *Inorg. Chem.* **2006**, *45*, 6565–6567.
(35) Ziessel, R.; Diring, S.; Retailleau, P. *Dalton Trans.* **2006**, 3285–3290.
(36) Grosshenny, V.; Romero, F. M.; Ziessel, R. *J. Org. Chem.* **1997**, *62*, 1491–1500.

(DMF; 3 mL) and triethylamine (1 mL) followed by the addition of 4-ethynyl-2,2′:6′,6″-terpyridine (0.063 g, 0.244 mmol). The solution was vigorously degassed by bubbling argon through the solution. The addition of CuI (1.0 mg, 0.005 mmol) to the yellow solution resulted in an instantaneous color change to red. After stirring at room temperature overnight, the deep-red solution was concentrated to 1 mL, filtered over Celite, and dropped into an aqueous solution of $NaBF_4$ (1.200 g/10 mL). The complex was recovered by filtration over paper and washed with water (3 × 100 mL), and the red solid was dried under high vacuum. Purification was ensured by column chromatography using alumina as the solid support and a gradient of methanol (0−1%) in dichloromethane as the mobile phase. Ultimate recrystallization by slow evaporation of dichloromethane from a dichloromethane/hexane solution afforded complex **1** (0.202 g, 88%). ^{1}H NMR (200.1 MHz, $CDCl_3$): δ 9.12 (d, ^3J = 6.0 Hz, 2H), 8.97 (s, 2H), 8.96 (s, 2H), 8.89 (d, ^3J = 8.0 Hz, 4H), 8.69 (dm, ^3J = 4.8 Hz, 1H), 8.61 (d, ^3J = 8.0 Hz, 1H), 8.47 (s, 2H), 7.87 (td, ^3J = 8.0 Hz, ^4J = 1.9 Hz, 1H), 7.60 (m, 2H), 7.34 (m, 1H), 1.65 (s, 9H), 1.52 (s, 18H). UV−vis (CH_2Cl_2): λ, nm (ε, M^{-1} cm^{-1}) 410 (7600), 336 (21 700), 311 (27 100), 285 (66 200). FT-IR (KBr): ν 3338 (m), 2960 (m), 2122 (m, $\nu_{C\equiv C}$), 1614 (s), 1582 (s), 1563 (s), 1466 (s), 1392 (m), 1261 (m), 880 (m), 792 (m). ES-MS: *m*/*z* 852.4 (100%, $[M - BF_4]^+$) in CH_2Cl_2. Anal. Calcd for $C_{44}H_{45}N_6PtBF_4$ (M_r = 939.75): C, 56.24; H, 4.83; N, 8.94. Found: C, 55.75; H, 4.62; N, 8.63.

[Fe(ᵗBu₃tpyPtC≡Ctpy)₂](ClO₄)₄ (2). Compound **1** (0.064 g, 0.066 mmol) was dissolved in methanol (10 mL) and vigorously degassed with argon. $Fe(ClO_4)_2 \cdot 6H_2O$ (0.012 g, 0.032 mmol) was added as a solid under argon, resulting in an instantaneous color change to deep violet. A deep-violet precipitate formed after 10 min of stirring. After 4 h, the resulting precipitate was recovered by centrifugation and washed with cold methanol and diethyl ether. Anion exchange was ensured by dissolution of the crude complex in DMF (5 mL) and dropwise addition to an aqueous solution of $LiClO_4$ (20 equiv). The precipitate was collected by centrifugation and washed with water, methanol, and diethyl ether. Recrystallization was achieved by slow evaporation of acetone from a mixture of acetone/cyclohexane. Complex **2** was isolated as a deep-violet crystalline solid (0.0627 g, 88% yield). ^{1}H NMR ($(CD_3)_2CO$, 400 MHz): δ 9.50 (d, 4H, ^3J = 6.0 Hz), 9.20 (s, 4H), 8.89 (s, 4H), 8.50 (d, 4H, ^4J = 2.2 Hz), 8.81 (d, 4H, ^3J = 8.0 Hz), 8.12 (dd, 4H, J = 6.0 and 2.2 Hz), 8.04 (td, 4H, J = 7.7 and 1.1 Hz), 7.55 (d, 4H, ^3J = 5.4 Hz), 7.32−7.28 (m, 4H), 1.58 (s, 18H), 1.54 (s, 36H). UV−vis (CH_2Cl_2): λ, nm (ε, M^{-1} cm^{-1}) 584 (30 900), 425 (sh, 9900), 375 (22 400), 312 (73 900), 288 (110 200), 266 (86 600). FT-IR (KBr): ν 2957 (m), 2911 (m), 2866 (m), 2099 (m, $\nu_{C\equiv C}$), 1605 (s), 1467 (s), 1424 (s), 1408 (s), 1365 (m), 1257 (m), 1103 (s). ES-MS: *m*/*z* 620.2 (100%, $[M - 3ClO_4]^{3+}$), 440.3 (30%, $[M - 4ClO_4]^{4+}$) in methanol/acetonitrile. Anal. Calcd for $C_{88}H_{90}N_{12}Pt_2FeCl_4O_{16}$ (M_r = 2159.54): C, 48.94; H, 4.20; N, 7.78. Found: C, 48.72; H, 4.00; N, 7.57.

[Zn(ᵗBu₃tpyPtC≡Ctpy)₂](ClO₄)₄ (3). The same procedure as that for complex **2** was followed, using $Zn(ClO_4)_2 \cdot 6H_2O$ instead of $Fe(ClO_4)_2 \cdot 6H_2O$. Complex **3** was isolated as a pale-yellow crystalline solid (0.066 g, 92% yield). ^{1}H NMR ($(CD_3)_2CO$, 300 MHz): δ 9.31 (d with ^{195}Pt satellites, 4H, ^3J = 5.7 Hz), 8.97 (d, 4H, ^3J = 4.5 Hz), 8.92 (d, 4H, ^3J = 7.9 Hz), 8.74 (s, 4H), 8.70 (s, 4H), 8.66 (d, 4H, ^4J = 1.9 Hz), 8.26 (td, 4H, J = 7.8 and 1.6 Hz), 8.21 (dd, 4H, J = 6.0 and 2.1 Hz), 7.89−7.85 (m, 4H), 1.54 (s, 18H), 1.46 (s, 36H). UV−vis (CH_2Cl_2): λ, nm (ε, M^{-1} cm^{-1}) 428 (12 800), 375 (24 200), 287 (110 000), 268 (76 900). FT-IR (KBr): ν 2963 (m), 2954 (m), 2916 (m), 2847 (m), 2097 (m, $\nu_{C\equiv C}$), 1607 (s), 1474 (s), 1429 (s), 1412 (s), 1367 (m), 1262 (m), 1257 (m), 1102 (s). ES-MS: *m*/*z* 623.2 (100%, $[M - 3ClO_4]^{3+}$), 442.5 (20%, $[M - 4ClO_4]^{4+}$) in methanol/acetonitrile. Anal. Calcd for $C_{88}H_{90}N_{12}Pt_2ZnCl_4O_{16}$ (M_r = 2169.09): C, 48.73; H, 4.18; N, 7.75. Found: C, 48.49; H, 4.02; N, 7.56.

Titration of 1 with Fe(ClO₄)₂. A 221.9 μM solution of $Fe(ClO_4)_2 \cdot 6H_2O$ and a 17.0 μM solution of **1** were prepared in CH_2Cl_2. Absorption and emission spectra were recorded simultaneously after each addition of Fe^{II}. The titration was stopped after no more changes were observed in the absorption and emission properties. All emission spectra and intensity decays were measured using the lowest energy isosbestic point available in the absorption spectrum.

Titration of 1 with Zn(ClO₄)₂. For this experiment, a 220 μM solution of $Zn(ClO_4)_2 \cdot 6H_2O$ and a 10.2 μM solution of **1** were prepared in CH_2Cl_2. Absorption and emission spectra were measured after each addition of Zn^{II}, and the titration was stopped when the spectral changes remained constant upon the addition of further aliquots. All emission spectra and intensity decays were measured using the lowest energy isosbestic point available in the absorption spectrum.

Time-Dependent Theory. The emission spectra are calculated using the fundamental equation in time-dependent theory.[37–45]

$$I(\omega) = C\omega^3 \int_{-\infty}^{+\infty} \exp(i\omega t)\left\{\langle\Phi|\Phi(t)\rangle \exp\left(-i\frac{E_0}{h}t - \Gamma^2 t^2\right)\right\} \mathrm{d}t \quad (1)$$

where $I(\omega)$ is the intensity of emission in photons per unit of volume per unit of time at frequency ω, C is a constant, E_0 is the energy difference between the minima of the excited and ground states, and Γ is a damping factor, which comes from the relaxation into other modes and the "bath".[37] In eq 1, the total autocorrelation function term $\langle\Phi|\Phi(t)\rangle$ is the overlap between the initial wave packet, Φ, and the time-dependent wave packet, $\Phi(t)$. In a one-coordinate system and with the assumption that the potential surfaces are harmonic, the force constants are kept the same between the ground and excited states, and the transition dipole moment is a constant (Condon approximation), the total autocorrelation function can be calculated by[37]

$$\langle\Phi|\Phi(t)\rangle = \exp\left\{-\frac{\Delta^2}{2}[1 - \exp(-i\omega_v t)] - \frac{i\omega_v t}{2}\right\} \quad (2)$$

where ω_v is the vibrational frequency in cm^{-1} and the dimensionless distortion Δ is the displacement of the normal mode. In the current work, ω_v used in the spectral fitting was determined from the vibrational progression measured in the 77 K emission spectra, 1360 cm^{-1}, and the distortion parameter was varied to yield the best fit to the experimental data.

Spectroscopic Measurements. UV−vis absorption spectra were measured with a Cary 50 Bio spectrophotometer accurate to ±2 nm. Uncorrected luminescence spectra were recorded on a PTI Instruments spectrofluorimeter (QM-4/2006-SE) equipped with a

(37) Zink, J. I.; Shin, K.-S. K. *Adv. Photochem.* **1991**, *16*, 119–214.
(38) Lee, S.-Y.; Heller, E. J. *J. Chem. Phys.* **1979**, *71*, 4777–4788.
(39) Heller, E. J. *Acc. Chem. Res.* **1981**, *14*, 368–375.
(40) Heller, E. J.; Sundberg, R. L.; Tannor, D. J. *J. Phys. Chem.* **1982**, *86*, 1822–1833.
(41) Hanna, S. D.; Zink, J. I. *Inorg. Chem.* **1996**, *35*, 297–302.
(42) Wootton, J. L.; Zink, J. I. *J. Phys. Chem.* **1995**, *99*, 7251–7257.
(43) Reber, C.; Zink, J. I. *J. Chem. Phys.* **1992**, *96*, 2681–2690.
(44) Henary, M.; Wootton, J. L.; Khan, S. I.; Zink, J. I. *Inorg. Chem.* **1997**, *36*, 796–801.
(45) Henary, M.; Zink, J. I. *J. Am. Chem. Soc.* **1989**, *111*, 7407–7411.

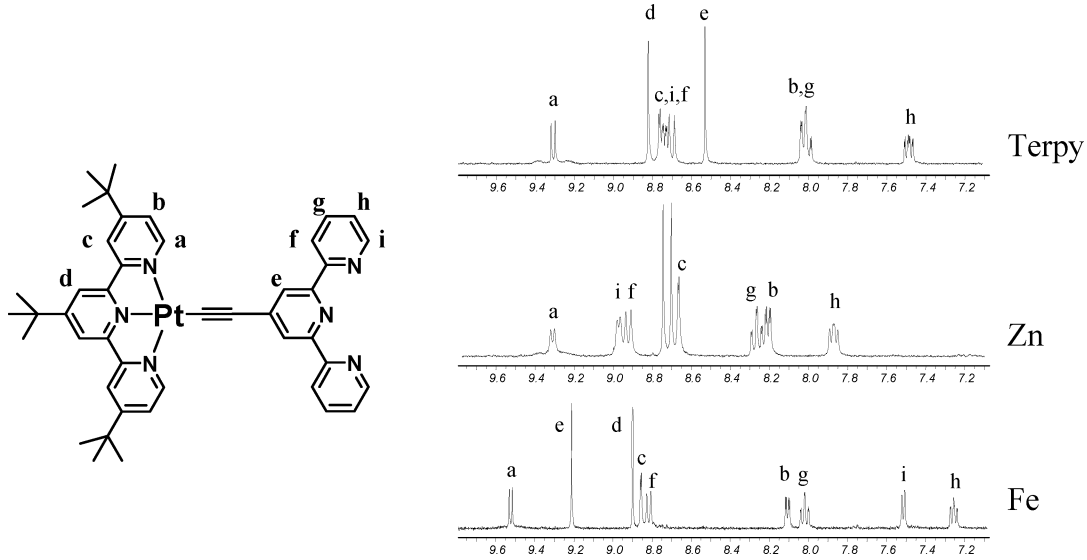

Figure 1. ^{1}H NMR in acetone-d_6 at 300 MHz for complexes **1**−**3**. To ensure adequate solubility, hexafluorophosphate was used as the counterion.

75 W xenon lamp as the excitation source and a R-928 PMT detector for the UV−vis region. For detection of singlet oxygen in the near-IR region, a Coherent Innova 306 argon ion laser was used as the excitation source in conjunction with a Peltier cooled InGaAs detector with lock-in amplification; the detector was mounted to the exit port of a second monochromator integrated into the PTI system. All of the photophysical experiments were performed using optically dilute solutions (OD = 0.08−0.1) in spectroscopic-grade solvents, and the samples contained in 1 cm^2 anaerobic quartz cells (Starna Cells) were deoxygenated with solvent-saturated argon for at least 45 min prior to measurement. For detection of singlet oxygen, the samples were purged with pure oxygen gas for 2 min prior to data acquisition. The 77 K spectral data were collected on a single-photon-counting spectrofluorimeter from Edinburgh Analytical Instruments (FL/FS 900). Emission lifetimes were measured by means of a nitrogen-pumped broad-band dye laser (2−3 nm fwhm; PTI GL-3300 nitrogen laser, PTI GL-301 dye laser, C-450 dye) using the experimental apparatus previously described.[17] PL quantum yields were determined using $[Ru(bpy)_3]^{2+}$ in argon-saturated CH_3CN ($\Phi_{em} = 0.062$)[46] as the quantum counter.

Time-resolved emission spectra were acquired in argon-saturated CH_2Cl_2 solutions and EtOH/MeOH matrixes at 77 K, using a computer-controlled Nd:YAG laser Quantel/OPO system from OPOTEK tuned at 430 nm for the measurements at room temperature and at 410 nm for the measurements at 77 K. A Micro HR Horiba/JY spectrograph equipped with a 300 g/mm grating interfaced with an Andor iSTAR iCCD served as the detection system. Typical experiments employed a gate width of 100 ns at room temperature and of 1 μs at 77 K averaged over 200 laser shots.

Results and Discussion

All complexes were thoroughly characterized by NMR in solution (Figure 1), and the assignment of the terpyridine (tpy) peaks was achieved on the basis of 2D NMR studies (Figures S3−S6 in the Supporting Information). The ^{1}H NMR spectra of Zn^{II} and Fe^{II} are typical of bisterpyridine-metal(II) complexes in an octahedral environment, inducing a magnetic equivalence of the two ligands resulting from a 2-fold symmetry axis lying along the Pt−M−Pt main axis. For each complex, the deshielded signal can safely be attributed to protons a, the closest to the nitrogen atoms of the platinum terpyridine subunit, easily identified by their ^{195}Pt satellites. In the same manner, protons h, which are in the meta position of the nonsubstituted pyridines, can be identified as the most shielded signals. Protons c are characterized by a weakly coupling doublet (^4J) around 8.80 ppm and are affected slightly when the metal chelates free the tpy. This is also the case for protons f, b, and g. One noteworthy effect upon complexation of the free tpy subunit is a downfield shift of protons e caused by the electron-withdrawing effect of the chelated metal. Note that this shift is much stronger in the case of the Fe^{II} complex (from 8.52 to 9.21 ppm), which is even less shielded than the singlet (8.90 ppm) referring to the platinum terpyridine fragment. The most striking effect is the shielding of the doublet attributed to protons i, from 8.75 in complex **1** to 7.51 ppm in complex **2** when the free tpy fragment is complexed with iron. Coordination resulted in an all-cis conformation of the nitrogen atoms and a stiffening of the tpy fragment. This forces the protons i, ortho to the nitrogen atoms of the external pyridines, into the shielding zone of the central pyridine on the opposite tpy. In the case of the Zn^{II} complex, protons i are slightly downshifted (from 8.75 to 8.97 ppm) upon zinc complexation. This effect has previously been discussed in related compounds and is likely due to the Lewis acidity of the Zn^{II} metal center.[47] Indeed, for the latter, protons i are slightly downshifted (from 8.75 to 8.97 ppm) upon zinc complexation. Finally, the protons d and e were safely assigned owing to a pronounced NOESY effect with the *tert*-butyl substituents (Figure S4 in the Supporting Information). For complex **3**, firm assignments for the protons d and e are impossible because of the weak shift observed.

The absorption and steady-state PL spectra of compound **1** are displayed in Figure 2. As most other platinum(II) terpyridylacetylide complexes, the bands in the region between 250

(46) Caspar, J. V.; Meyer, T. J. *J. Am. Chem. Soc.* **1983**, *105*, 5583–5590.

(47) Tessore, F.; Roberto, D.; Ugo, R.; Pizzotti, M. *Inorg. Chem.* **2005**, *44*, 8967–8978.

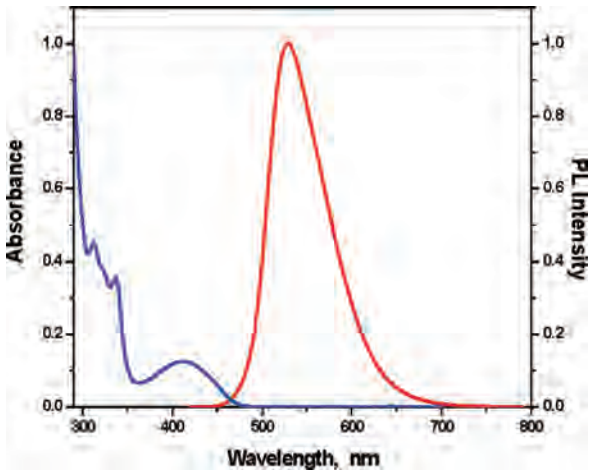

Figure 2. Absorption (blue line) and PL (red line) spectra of compound **1** in CH_2Cl_2.

and 350 nm are assigned to $^1\pi-\pi^*$ transitions localized on the terpyridyl ligand and the low-energy absorption band is assigned to charge-transfer (CT) transitions that are mainly metal-to-ligand (ML) in nature but with important contributions from the acetylenic π orbitals into the highest occupied molecular orbital (HOMO) levels.[1,3,11–13,19] Complex **1** displays an intense luminescence in dichloromethane, with a broad emission profile, consistent with CT parentage, with $\lambda_{max} = 529$ nm and a luminescence quantum yield of 0.20. The excited-state lifetime of complex **1** is 2.17 μs (single exponential) at room temperature in CH_2Cl_2. In coordinative solvents like acetonitrile, a dynamic quenching of the PL is observed and this phenomenon will be described in a future publication. Table 1 collects all photophysical data from **1**−**3** along with protonated **1** determined in the present study, and where possible calculated values of k_r and k_{nr} are included. In all instances, the values of k_r and k_{nr} support a triplet CT-based parentage for the emitting excited states in **1**, **3**, and protonated **1**; the specific details are provided below.

The presence of dissolved dioxygen in the CH_2Cl_2 solutions efficiently quenches the emission emanating from complex **1**, supporting the presence of a triplet-based excited-state emissive manifold. This preliminary result was corroborated by the ability of this complex to sensitize $^1O_2$ PL in the near-IR at 1270 nm (Figure S7 in the Supporting Information) in CH_2Cl_2.[48–50]

Because **1** has a free chelation site on the pendant terpyridyl unit, attachment of metal ions is possible, with potential modification of the photophysics of the initial Pt^{II} complex. Upon addition of Fe^{II} to a solution of **1** in CH_2Cl_2, a new band at 583 nm was observed, which is readily assigned to a $Fe^{II} \rightarrow$ tpy CT transition[33,34] (Figure 3). Two clearly resolved isosbestic points at 412 and 448 nm were observed as well (Figure 3a). The CT band corresponding to the Pt^{II} system blue-shifted upon Fe^{II} coordination, going from 415 to 383 nm, with an incremental increase in its absorbance. The observed blue shift in the CT absorption band can be attributed to the fact that, upon chelation of Fe^{II}, a Lewis acid, the HOMO orbital is stabilized relative to **1**, thereby increasing the energy of the associated transitions.[19,51–53] The bands corresponding to the $\pi-\pi^*$ transitions also increased in intensity upon chelation to Fe^{II}. Addition of Fe^{II} to a solution of **1** in CH_2Cl_2 induced a static quenching of the emission profile at 529 nm (Figure 3b), suggesting that, upon coordination of Fe^{II}, the ligand field and other low-energy states present readily afford deactivation of the excited states by nonradiative pathways. The absorption and emission properties were also measured on the pure isolated compound (**2**), quantitatively matching the results obtained on the extreme of the titration.

To determine how the coordination of the pendant terpyridyl unit affects the energy levels of the ligand, the titration experiment was also performed with Zn^{II}, which will permit the planarization of the terpyridyl ligand in addition to providing the octahedral coordination environment of Fe^{II} without producing a myriad of low-energy deactivating states. Upon addition of Zn^{II}, the CT band of complex **1** blue-shifted, increasing its intensity at 407 nm. We attribute the blue shift to the Lewis acidity of Zn^{II}, which in essence stabilizes the HOMO levels relative to the "free" tpy complex **1**. We note that an identical blue shift is observed when excess $HClO_4$ is added to a CH_2Cl_2 solution of **1**, thereby simulating the influence of acid on the nonbonding electrons resident on the terpyridylacetylide nitrogen atoms (Figure S10a in the Supporting Information). This behavior has been observed previously in analogous amine-substituted acetylide complexes of Pt^{II}.[19,51–53] As expected from the electrochemical inaccessibility of the Zn^{II} metal center, no additional bands were formed in the absorption spectrum during the titration, and the formation of an isosbestic point at 428 nm was observed (Figure 4a). Even though quenching of the emission at 529 nm was observed throughout the titration experiment, the new Pt−Zn−Pt complex (**3**) formed was emissive under the conditions used, with $\lambda_{max} = 491$ nm and a shoulder at 519 nm (isoemissive point at 497 nm; Figure 4b). This emission spectrum was also measured in the isolated compound (**3**), which exhibits the same emission profile as that observed in the titration product. The addition of excess $HClO_4$ to **1** results in the generation of an emission profile that is identical with that measured for **3** (Figure S10b in the Supporting Information) with a somewhat enhanced quantum efficiency of 0.07. Once again, the only significant role that coordinated Zn^{II} seems to play is that of a Lewis acid, which serves to stabilize the HOMO levels, producing a higher energy emission spectrum that remains CT in nature.

The luminescence quantum yield of complex **3** is 0.03, and the excited-state lifetime decay is 215 ns in CH_2Cl_2 at room temperature. The combined photophysics observed from this chromophore are most consistent with a CT-based excited state. In contrast to compound **1**, the HOMO in **3**

(48) Bromberg, A.; Foote, C. S. *J. Phys. Chem.* **1989**, *93*, 3968–3969.
(49) Mulazzani, Q. G.; D'Angelantonio, M.; Venturi, M.; Rodgers, M. A. J. *J. Phys. Chem.* **1991**, *95*, 9605–9608.
(50) Muro, M. L.; Castellano, F. N. *Dalton Trans.* **2007**, 4659–4665.
(51) Han, X.; Wu, L.-Z.; Si, G.; Pan, J.; Yang, Q.-Z.; Zhang, L.-P.; Tung, C.-H. *Chem.—Eur. J.* **2007**, *13*, 1231–1239.
(52) Lu, W.; Chan, M. C. W.; Zhu, N.; Che, C. M.; He, Z.; Wong, K. M.-C. *Chem.—Eur. J.* **2003**, *9*, 6155–6166.
(53) Yam, V. W.-W.; Hui, C.-K.; Yu, S.-Y.; Zhu, N. *Inorg. Chem.* **2004**, *43*, 812–821.

Table 1. Photophysical Properties of Compounds **1**−**3**

compound	λ_{abs}, nm	λ_{em}, nm	Φ_{em}[c]	τ_{em},[c] μs	k_{nr}[d] ($\times 10^5$) s^{-1}	k_r[e] ($\times 10^4$) s^{-1}
1	284, 312, 336, and 415[a]	529;[a] 474, 506, and 546[b]	0.20	2.17;[a] 8.3[b]	3.69	9.22
2	286, 312, 329, 383, and 583[a]					
3	286, 309, 330, and 407[a]	491 and 519;[a] 474, 506, and 546[b]	0.03	0.215;[a] 8.6[b]	44.9	15.8
1 + $HClO_4$	289, 312, 335, and 408[f]	491 and 519;[f] 474, 506, and 546[b]	0.07	0.722 and 0.249;[f] 8.3[b]	15.0	11.3

[a] Measured in an argon-saturated CH_2Cl_2 solution at room temperature. [b] Measured at 77 K in a 4:1 EtOH/MeOH matrix. [c] PL quantum yields and lifetime decays, ±5%. [d] $k_{nr} = (1 - \Phi)/\tau$. [e] $k_r = \Phi/\tau$. [f] Measured after an excess (8.82×10^{-2} μmol, 74 μL) of $HClO_4$ (1.2×10^{-3} M) was added to a 6.2 μM solution of **1** in an argon-saturated CH_2Cl_2 solution at room temperature.

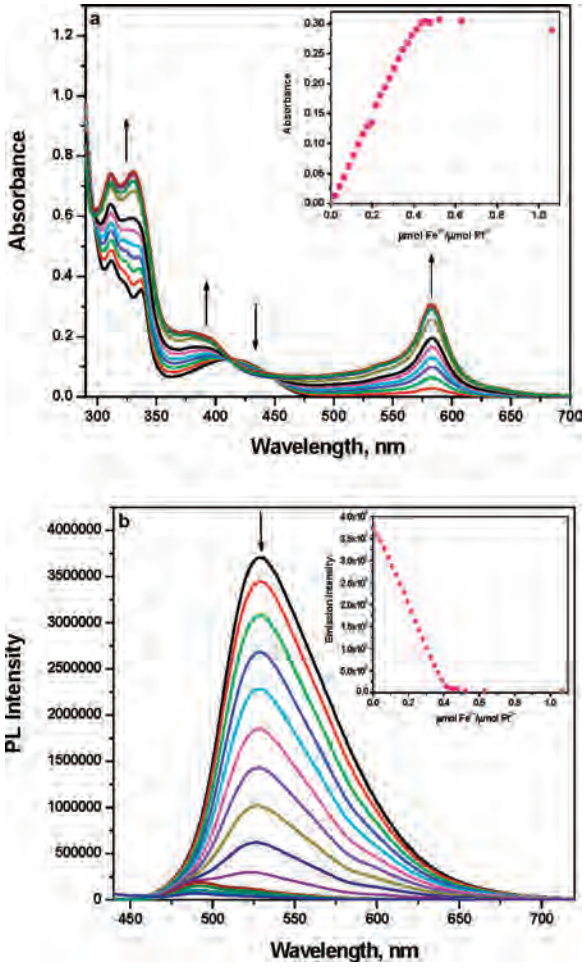

Figure 3. Titration of **1** with Fe^{II} followed by absorption (a) and PL (b) changes. The insets show the change in absorbance at 583 nm (a) and emission at 529 nm (b) as a function of μmol of Fe^{II}/μmol of Pt^{II}. No further spectroscopic changes were observed beyond 0.5 equiv (stoichiometric point) of Fe^{II} added.

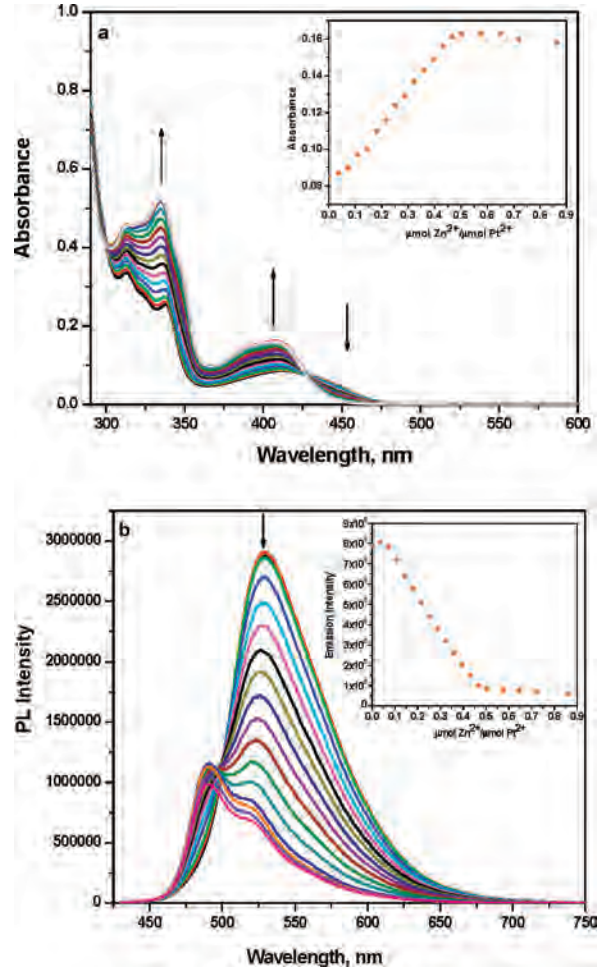

Figure 4. Titration of **1** with Zn^{II} followed by absorption (a) and PL (b) changes. The insets show the change in absorbance at 407 nm (a) and emission at 600 nm (b) as a function of μmol of Zn^{II}/μmol of Pt^{II}. No further spectroscopic changes were observed beyond 0.5 equiv (stoichiometric point) of Zn^{II} added.

likely exhibits less terpyridylacetylide character [i.e., less ligand-to-ligand (LL) CT character] by comparison because the lifetime of the CT state has substantially shortened, the quantum yield has greatly decreased, and the emission profile now exhibits a low-energy shoulder.[19,51–53] Any significant electronic perturbation imparted by Zn^{II} (beyond Lewis acid effects) can be ruled out because the reaction of excess $HClO_4$ with **1** produces photophysics (and absorption features) similar to those measured for **3** (Figure S10 in the Supporting Information), even at 77 K (see Figure 6). The spectroscopic similarities suggest that the terpyridylacetylide subunit is providing a similar σ-donor environment (less electron-donating) for the Pt^{II} center in both instances. Because this influence would significantly impact the energies of MLCT-based transitions, we conclude that there is more MLCT character in protonated **1** and **3** than there is in the free base **1**. The time-resolved PL intensity decay of protonated **1** in CH_2Cl_2 is provided as Figure S11 in the Supporting Information. Even in the presence of excess acid, the intensity decay is complex and is most adequately modeled using a sum of two single exponential functions. In order to calculate k_r and k_{nr} values for protonated **1**, we used the average lifetime [$\tau = (\alpha_1\tau_1^2 + \alpha_2\tau_2^2)/(\alpha_1\tau_1 + \alpha_2\tau_2)$] for τ (619 ns) in this instance for both expressions in Table 1.[54] As in the case of **3**, the photophysical data of protonated **1** appear most consistent with a CT emission. Even though dissolved oxygen dynamically quenches the emission of **3**,

(54) Lakowicz, J. R. *Principles of Fluorescence Spectroscopy*, 3rd ed.; Springer: New York, 2006; p 142.

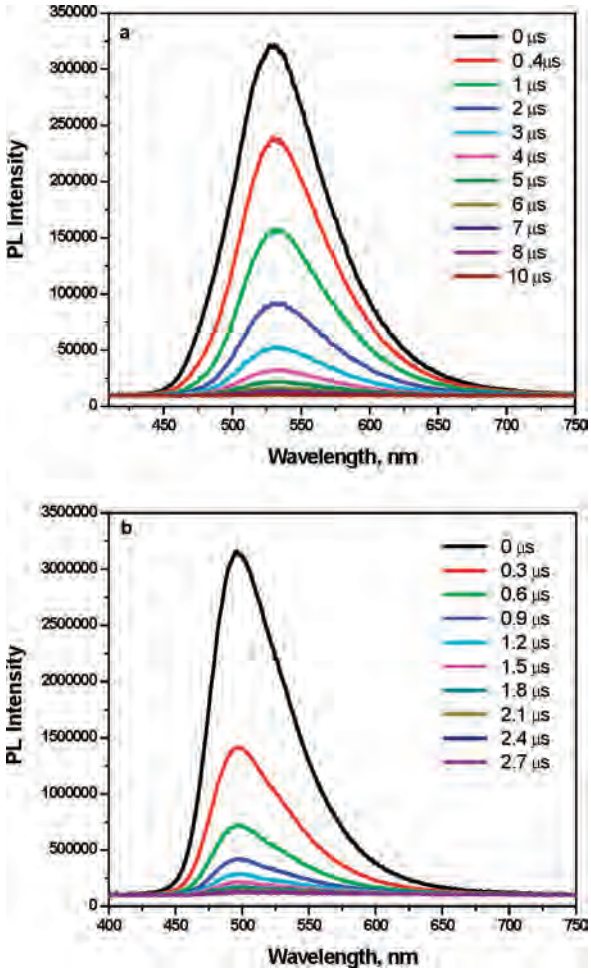

Figure 5. Time-resolved emission spectra measured for compounds **1** (a) and **3** (b) in dichloromethane at room temperature, $\lambda_{ex} = 430$ nm.

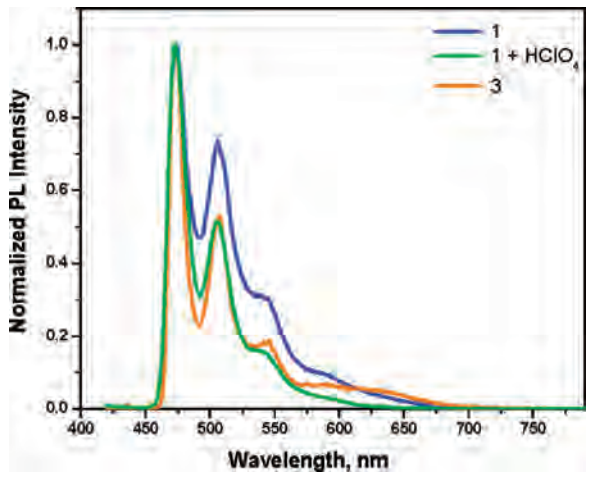

Figure 6. Comparison of the emission profiles of compounds **1** (blue line) and **3** (orange line) and the product of the acid titration of **1** with excess $HClO_4$ (green line) in 4:1 EtOH/MeOH matrixes at 77 K.

the process is not as efficient as that in the case of **1** and is attributed to the significantly shorter-lived excited state in **3**. The triplet nature of the CT excited state in **3** was further demonstrated by the generation of $^1O_2$ PL in the near-IR upon 442 nm visible light excitation of this complex in the presence of dissolved dioxygen (Figure S7 in the Supporting Information).

Time-resolved emission spectra were measured for compounds **1** and **3** in argon-saturated CH_2Cl_2 solutions at room temperature (Figure 5). For compound **1**, a symmetric decay of the emission profile with time was observed, suggesting the presence of just one kinetically relevant species producing the PL observed. For compound **3**, the main peak decays symmetrically with time, but after 2 μs, a second component is clearly observed. However, this feature represents a tiny fraction (<2%) of the total intensity decay profile (Figure 5b) and is therefore not worthy of additional discussion. In the steady-state spectrum, it is possible to observe a peak at 490 nm, but there is also a pronounced shoulder at 519 nm that matches the wavelength where the long-lived component is observed in the time-resolved experiment.

Figure 6 displays the emission spectra recorded for **1**, protonated **1**, and **3** at 77 K. Each complex displays a vibronically structured emission profile in the EtOH/MeOH glassy matrix with a concomitant blue shift in their emission bands relative to those observed at room temperature. The vibrational spacing of approximately 1300 cm^{-1} observed at 77 K (Figure 6) is consistent with the vibrational modes on the terpyridyl aromatic system (largely C═C and C═N in nature), which supports the notion of a ligand-localized emission at 77 K. Going from 298 to 77 K induces a marked increase in the excited-state lifetimes of compounds **1** and **3**. Interestingly, the single-exponential excited-state lifetimes at 77 K of these compounds are almost the same (8.3 μs for **1**, 8.6 μs for **3**, and 8.3 μs for protonated **1**), with a 3.8-fold increase for **1** and a 40-fold for **3**, in comparison to the room temperature data. This result in itself suggests that the nature of the emissive state at 77 K is likely the same in both complexes, which is consistent with a ligand-localized excited state. This observation is also congruent with the notion that the CT manifolds increase in energy from room temperature to 77 K, whereas ligand-localized triplet manifolds in both structures essentially remain fixed over the same temperature range. We note that even though the emission wavelengths of **1** and **3** substantially overlap, their relative intensities are quite different.

Another interesting observation to point out here is the ability for these complexes to produce aggregates with increasing chromophore concentration, a well-established phenomenon.[55,56] For high concentrations of the complexes in the low-temperature matrix, a structureless emission band is observed around 650 nm in both instances. Upon consecutive dilutions, the band in the red eventually disappears, revealing just the vibronic-structured emission profile seen in Figure 6 (Figure S8 in the Supporting Information).

Time-resolved emission experiments were also performed at low temperature on **1** and **3** (Figure S9 in the Supporting Information). In both cases, a structured emission profile was observed, resembling the steady-state PL spectrum. The differences in relative intensities are still observed in time-gated emission and, as in steady-state experiments, the profiles are superimposed. Both spectra decay symmetrically

(55) Bailey, J. A.; Hill, M. G.; Marsh, R. E.; Miskowski, V. M.; Schaefer, W. P.; Gray, H. B. *Inorg. Chem.* **1995**, *34*, 4591–4599.
(56) Yam, V. W.-W.; Wong, K. M.-C.; Zhu, N. *J. Am. Chem. Soc.* **2002**, *124*, 6506–6507.

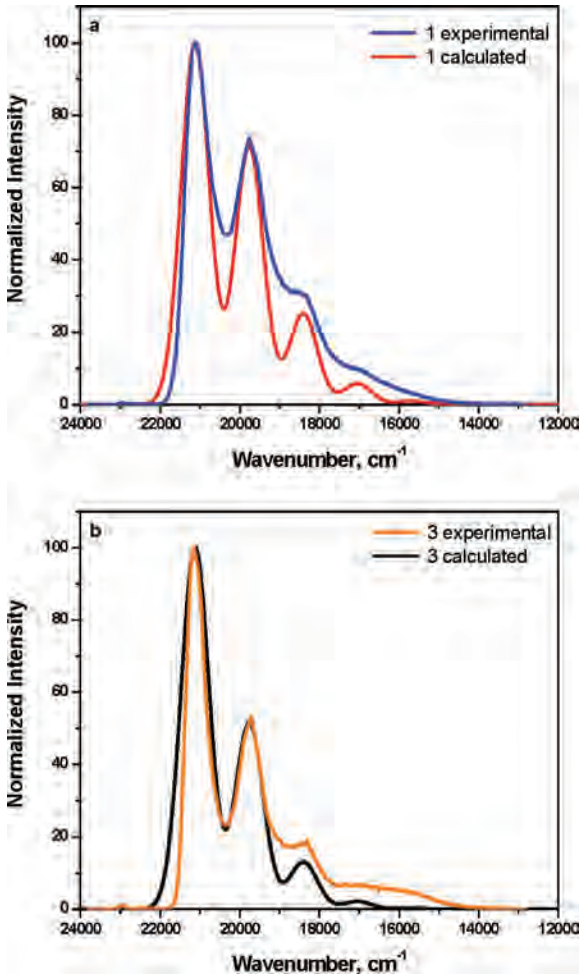

Figure 7. Calculated emission spectra of **1** (a) and **3** (b) at 77 K using the 1360 cm^{-1} mode compared to the experimental data from Figure 6.

with time, except for the region around 600 nm, which exhibits a shoulder that seems to decay faster than the remaining profile. This result is consistent with the presence of a small population of aggregates even at low concentrations of the metal complex in the low-temperature matrix. The kinetic data obtained in time-resolved emission spectral experiments quantitatively agree with the single-wavelength intensity decay measurements performed on our transient luminescence apparatus. According to the pooled results from above, the PL data observed at low temperature in **1** and **3** are emanating from the same ligand-localized excited state.

In order to further determine the nature of the excited states in these complexes, calculation of the emission profiles of **1** and **3** at low temperature was performed using time-dependent theory (Figure 7). The interval between the main and branch peaks is 1360 cm^{-1}, which was used as the vibrational frequency (ω_v) in the calculation, $E_0 = 21\,100$ cm^{-1} was determined from the main (origin) peak of the emission spectra, and the damping factor Γ was chosen to give an appropriate fit to the width of the experimental peaks (250 cm^{-1} for compounds **1** and **3**). The dimensionless distortion Δ is fitted from the relative intensity between the main and branch peaks; 1.12 and 1.32 are used in fitting the emission spectra of **3** and **1**, respectively. The different dimensionless distortions likely result from slightly different geometries of the upper triplet ligand-centered electronic state, which implies that the ligand-localized triplet state is centered on the terpyridylacetylide fragment. Because the 1360 cm^{-1} mode is assigned to the tpy ring deformation mode involved in the C═C stretch[57] and the excited state is most likely localized on the terpyridylacetylide ligand, the different dimensionless distortions imply that the tpy C═C and C═N bond lengths of the upper triplet ligand-centered electronic state vary slightly between each molecule.

(57) Schneider, S.; Brehm, G.; Jager, W.; Silva, M. I.; Burrows, H. D.; Formosinho, S. T. *J. Raman Spectrosc.* **1996**, *27*, 163–175.

Conclusions

We have demonstrated that the Pt^{II} structure proposed here is not suitable for the production of long-lived Fe^{II}-containing transition-metal complexes. On the other hand, chelation of Zn^{II} to the pendant unit in the Pt^{II} system demonstrated that it is possible to go from a mononuclear system displaying emission from a ^{3}CT excited-state manifold to a trinuclear system possessing a higher energy ^{3}CT excited state with higher energy absorption features, shorter excited-state lifetime, and lower quantum efficiency. The behavior of protonated **1** strongly mimics the photophysics of **3**; therefore, the chelation of Zn^{II} to **1** and the resultant electronic effects simply result from its Lewis acidity, stabilizing the HOMO levels, thereby producing the combined chromophore properties described above. The combined room temperature data suggest that the excited state is primarily composed of MLCT character in protonated **1** and **3**, whereas the composition in free base **1** is more of a composite, i.e., MLCT/LLCT. At 77 K, **1**, **3**, and protonated **1** all display similar emission energies, profiles, and lifetimes, suggesting that the same emitting state is attained in each structure, which is believed to be terpyridylacetylide ligand-localized in nature. Time-dependent theory calculations support this conclusion because the dimensionless distortion parameter obtained in each molecule suggests the origin of the emission is from similar, yet distinguishable ligand-localized parentages. Therefore, the spectral fitting also appears most consistent with the terpyridylacetylide ligand-localized excited state at 77 K, and molecules **1** and **3** exhibit inversion in their emitting states relative to room temperature.

Acknowledgment. F.N.C. acknowledges support from the Air Force Office of Scientific Research (Grant FA9550-05-1-0276), the National Science Foundation (Grant CHE-0719050), the ACS-PRF (44138-AC3), and the BGSU Research Enhancement Initiative. R.Z. acknowledges financial support from the CNRS and the ANR FCP-OLEDs 05-BLAN-0004-01. R.Z. also warmly thanks Johnson Matthey PLC for the loan of precious metals. We are indebted to Prof. Jeffrey I. Zink at UCLA for providing the necessary programs enabling our use of the time-dependent theory for emission spectral fitting.

Supporting Information Available: Additional NMR (COSY and NOESY correlations), PL, and singlet oxygen sensitization data. This material is available free of charge via the Internet at http://pubs.acs.org.

IC800316X